nature astronomy

SUPPLEMENTARY INFORMATION

DOI: 10.1038/s41550-017-0238-6

In the format provided by the authors and unedited.

Polarization due to rotational distortion in the bright star Regulus

Daniel V. Cotton[1]*, Jeremy Bailey[1], Ian D. Howarth[2], Kimberly Bott[3,4], Lucyna Kedziora-Chudczer[1], P. W. Lucas[5] and J. H. Hough[5]

[1]School of Physics, University of New South Wales, Sydney, New South Wales 2052, Australia. [2]Department of Physics and Astronomy, University College London, Gower Street, London WC1E 6BT, UK. [3]Virtual Planetary Laboratory, Seattle, WA 98195, USA. [4]Astronomy Department, University of Washington, Box 351580, Seattle, WA 98195, USA. [5]Centre for Astrophysics Research, School of Physics, Astronomy and Mathematics, University of Hertfordshire, Hatfield AL10 9AB, UK. *e-mail: d.cotton@unsw.edu.au

Polarization due to rotational distortion in the bright star Regulus

Daniel V. Cotton[1,*], Jeremy Bailey[1], Ian D. Howarth[2], Kimberly Bott[3,4], Lucyna Kedziora-Chudczer[1], P. W. Lucas[5], J. H. Hough[5]

[1]School of Physics, UNSW Sydney, NSW 2052, Australia.

[2]Department of Physics and Astronomy, University College London, Gower Street, London, WC1E 6BT, UK.

[3]Virtual Planetary Laboratory, Seattle, WA 98195, USA.

[4]University of Washington Astronomy Department, Box 351580, UW Seattle, WA 98195, USA.

[5]Centre for Astrophysics Research, School of Physics, Astronomy and Mathematics, University of Hertfordshire, Hatfield AL10 9AB, UK.

*Correspondence to: d.cotton@unsw.edu.au

Supplementary Information

Potential influence from Regulus' companions.

According to Gies et al.[49] Regulus has a companion star orbiting with a period of 40.11 days with a probable semi-major axis of 0.35 au – placing it at an angular separation of 0.014 arcsec, easily within the HIPPI and PlanetPol apertures, which are 6.7 and 5 arcsec respectively. The companion has a low mass (> 0.30 M_{Sun}) and is thought to be a white dwarf, but might also be a main-sequence M4 star.

If the companion is an M-dwarf the magnitude difference to the primary is thought to be equal to ~6 in the K-band[49]. A simple calculation assuming blackbody emission shows that, in this case, the companion would have to be polarized at more than 3000 ppm to contribute even 1 ppm to the overall signal in the most affected band (that being the PlanetPol band). No broadband linear-polarization measurements of M dwarfs have been made with modern equipment. A review of older measurements of red dwarfs given by Clarke[10] relates null detections even for very active stars like BY Dra. Recently we[28] have found active K dwarfs can be polarized, but only, so far, at low levels – up to around 50 ppm. Thus if the companion is an M dwarf we can quite confidently rule out any significant contribution from it.

If the companion is a white dwarf the magnitude difference in the K-band is given as ~10 by Gies et al.[49]. In this case the same calculation as above shows that the 425SP band is the one most likely to be effected; and an intrinsic contribution from the companion of ~2500 ppm would be required to change our measurement by 1 ppm. A recent R-band survey of non-magnetic white dwarfs[50] failed to make any 3-sigma detections, with a detection limit of typically ~5000 ppm. This gives us confidence that a significant intrinsic contribution from the companion is unlikely.

In addition to an intrinsic contribution from the companion itself, material entrained between the two stars could provide a scattering medium that would produce a non-zero signal. Any such signal would be variable on the timescale of the orbital period. We do not have data to specifically test this time-scale, however we regard it as unlikely, in large part because our repeat observations in multiple bands (as given in Supplementary Figure 5) demonstrate a high degree of consistency when considering the precision of the individual measurements.

The double star HD 87884 is also considered to be companion to Regulus, but at an angular separation of 175.94 arcsec[51] it is too distant to influence our observations.

The Öhman effect and inclination.

As a result of including the rotational Doppler shift in the polarized radiative transfer modeling, structure can be seen across spectral lines. Öhman[24] first inferred this result by analogy with Chandrasekhar's original modeling paper[1]. Much later, more quantitative results were obtained

by Collins & Cranmer[52]. They evaluated the effect for pure absorption spectral lines with a Struve-Unsöld model[53,54] that included limb darkening. For a B type star the magnitude of the effect was found to be 10s of ppm in *Q/I* for lines in the visible region of the spectrum, but much more than that in the UV[52]. Thus far the phenomenon has not been observed. If a high-precision spectro-polarimeter were to be turned to the task greater precision in determining inclination might be obtained. This is because the polarization in the spectral lines varies more strongly with inclination at high inclinations than does the broadband polarization. This can be seen in Supplementary Figure 6, where we show the region from 380 to 450 nm – where the greatest density of strong spectral lines is to be found – in both *U/I* and *Q/I* (where our results are of a similar magnitude to those of Collins & Cranmer in the visible region[52]). Particularly noteworthy is the rapid (positive and negative) increase in *U/I* away from 90 degrees inclination – up to 10 ppm in 10 degrees.

A comment on differential rotation.

As described earlier, all the modeling carried out here assumes rigid stellar rotation; this assumption is supported by conclusions in the literature that there is no significant surface differential rotation in early-type stars[23]. Yet, it is worth noting the possibility rapidly rotating early-type stars may not be rigid rotators[55,56]. Examining the effect of differential rotation on polarization is beyond the scope of this work. However, we have run models with and without Doppler velocities included to examine the Öhman effect, with no significant effect on the broadband polarization. Differential rotation will manifest in broadband polarization through changes in the latitudinal temperature distribution and the shape of the star. Both effects we expect to be modest, but we note that the approach we adopt here is well suited to investigating this question, since ultimately we are taking the sum of elements distributed over the disk of the star, and the stellar models representing each of these elements may be adjusted independently to correspond to a differential rotation model.

On the other hand, while line profiles aren't particularly sensitive to the shape of the star, they do map the distribution of temperature more directly than would the broadband polarization. As a consequence stellar spectral lines are a demonstrably better diagnostic of differential rotation[23].

Supplementary References

49 Gies, D. R. *et al.* A Spectroscopic Orbit for Regulus. *Astrophys. J. Lett.* **682**, L117-L120 (2008).

50 Żejmo, M., Słowikowska, A., Krzeszowski, K., Reig, P. & Blinov, D. Optical linear polarization of 74 white dwarfs with the RoboPol polarimeter. *Mon. Not. R. Astron. Soc.* **464**, 1294-1305 (2017).

51 Fabricius, C. *et al.* The Tycho double star catalogue. *Astron. Astrophys.* **384**, 180-189 (2002).

52 Collins, G. W., II & Cranmer, S. R. Rotationally induced polarization in pure absorption spectral lines. *Mon. Not. R. Astron. Soc.* **253**, 167-174 (1991).

53 Shajn, G. & Struve, O. On the rotation of stars. *Mon. Not. R. Astron. Soc.* **89**, 222-239 (1929).

54 Unsöld, A. *Physik der Sternatmosphären*. 508 (Springer-Verlag, Berlin, 1955).

55 Stoeckley, T. R. & Buscombe, W. Axial inclination and differential rotation for 19 rapidly rotating stars. *Mon. Not. R. Astron. Soc.* **227**, 801-813 (1987).

56 Zorec, J. *et al.* Critical study of the distribution of rotational velocities of Be stars. II: Differential rotation and some hidden effects interfering with the interpretation of the V sin i parameter. *Astron. Astrophys.* **602**, A83 (2017).

57 Hsu, J.-C. & Breger, M. On standard polarized stars. *Astrophys. J.* **262**, 732-738 (1982).

58 Martin, P. G., Clayton, G. C. & Wolff, M. J. Ultraviolet Interstellar Linear Polarization. V. Analysis of the Final Data Set. *Astrophys. J.* **510**, 905-914 (1999).

59 Wilking, B. A., Lebofsky, M. J., Kemp, J. C., Martin, P. G. & Rieke, G. H. The wavelength dependence of interstellar linear polarization. *Astrophys. J.* **235**, 905-910 (1980).

60 Johnson, H. L., Mitchell, R. I., Iriarte, B. & Wisniewski, W. Z. UBVRIJKL Photometry of the Bright Stars. *Comm. Lunar & Planetary Lab.* **4**, 99-110 (1966).

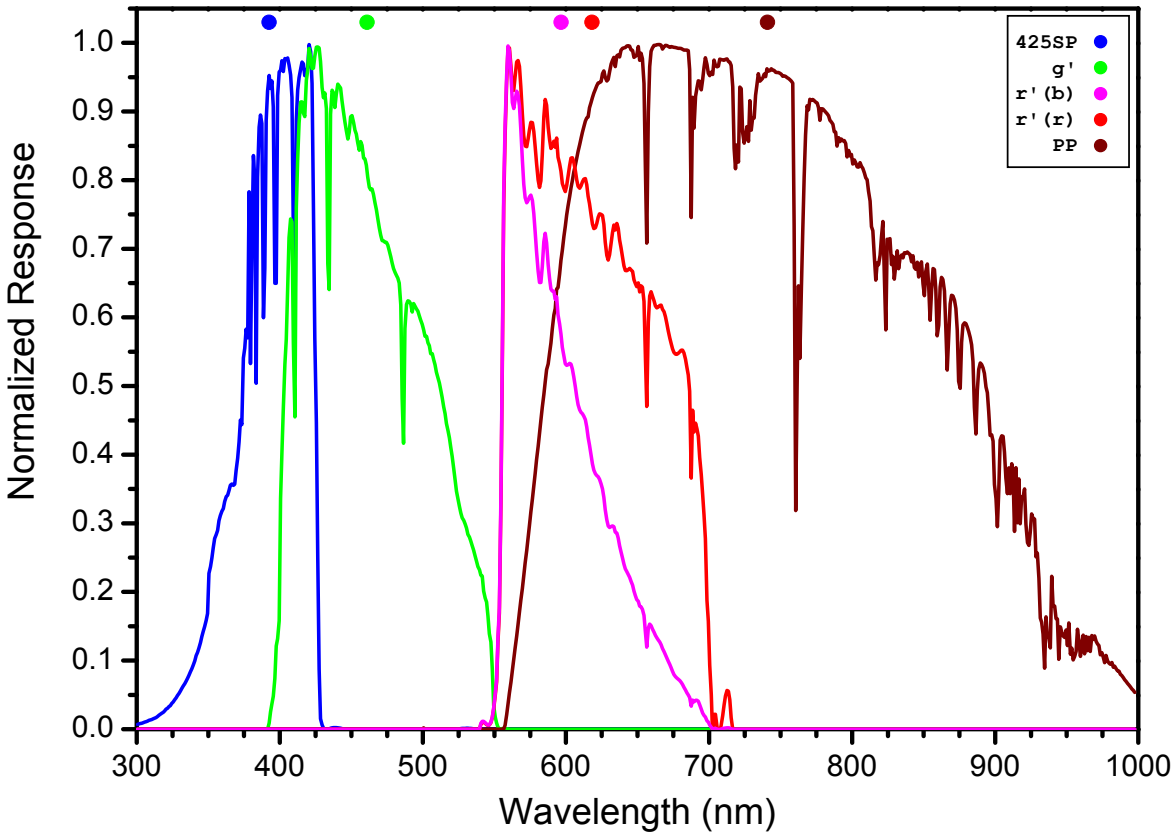

Supplementary Figure 1 | HIPPI and PlanetPol effective bandpasses.

The effective bandpasses used to observe Regulus. Colored dots, representing the effective wavelength of each band, are shown above a detailed normalized band response. The bandpass model begins with a model spectrum for Regulus with ω/ω_c = 0.95 and i = 90 degrees, and modifies the spectrum to take account of filter, detector and modulator responses as well as absorption by the atmosphere. The atmosphere model has been tailored for the observing sites of the AAT and WHT. An airmass of 1.0 was assumed, but higher airmasses result in negligible differences. The bandpass model is calculated with 0.01 nm resolution but has been binned per nanometer here.

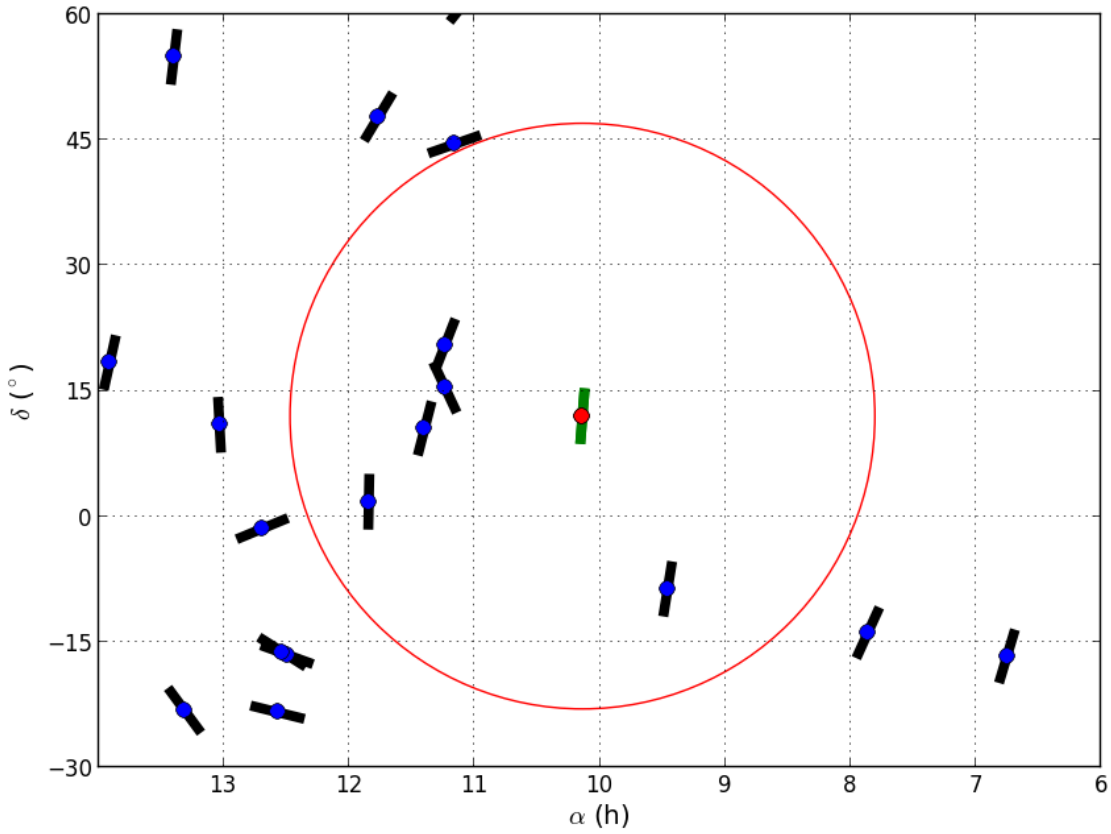

Supplementary Figure 2 | The determined interstellar polarization position angle of Regulus from nearby stars.

The red data point is Regulus, and the green bar its determined interstellar polarization position angle. The blue data points and black bars are nearby stars believed to be polarized only by the ISM and their position angles respectively. The plot shows the stars in right ascension (α) and declination (δ) with red circle denoting 35 degrees angular separation from Regulus, which represents the limit beyond which there is no correlation between the position angles of star pairs[28]. Position angle is defined in the range 0 – 180 degrees, and is measured anti-clockwise from 12 o'clock in the figure.

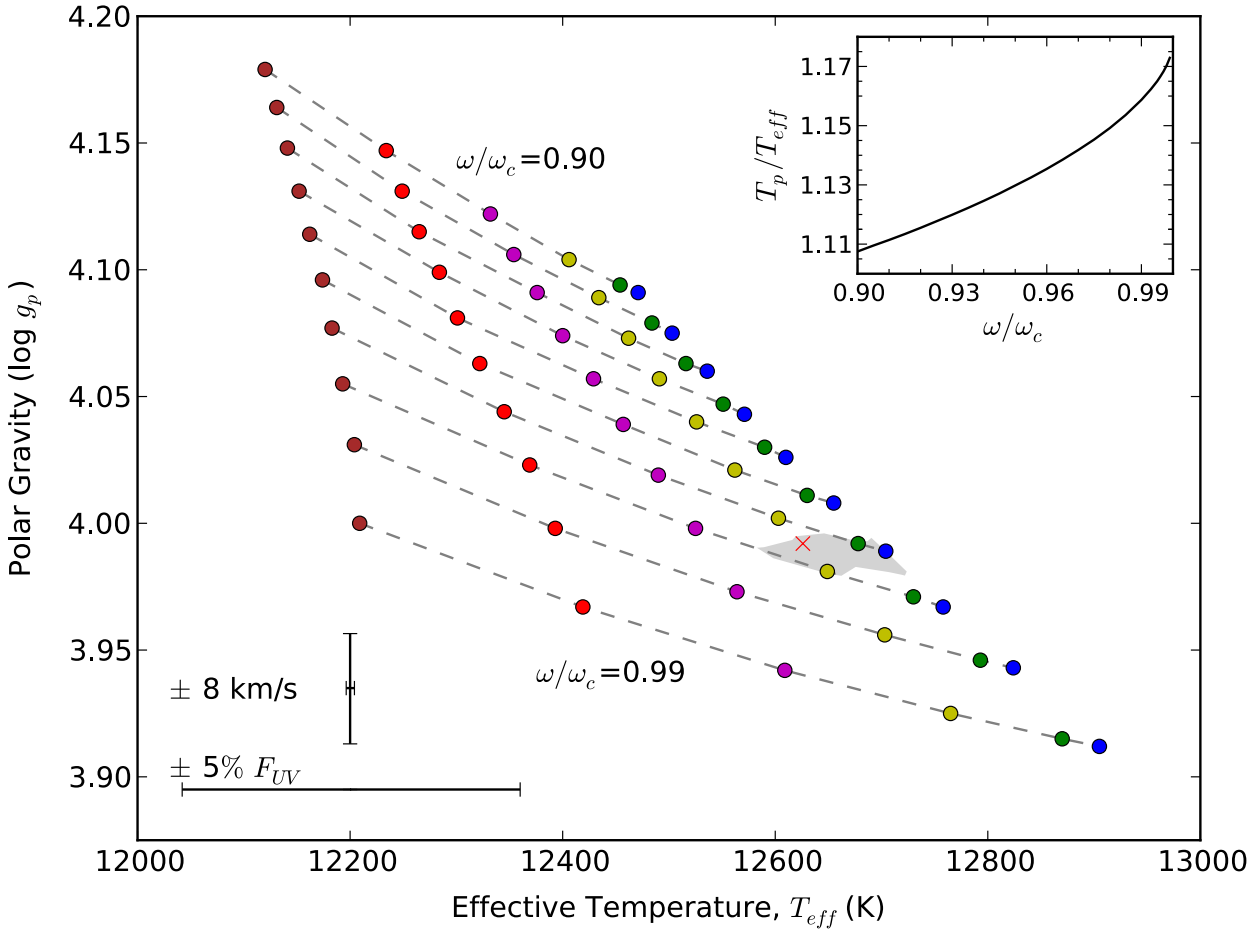

Supplementary Figure 3 | The initial grid of log g_p and T_{eff} generated from assumed values of ω/ω_c and *i*.

Running from brown to blue across the plot the colored dots represent inclinations of 65 to 90 degrees in 5 degree increments. Each dashed line corresponds to a line of constant ω/ω_c from 0.90 at the top of the plot to 0.99 at the bottom in increments of 0.01. Representative error bars associated with the measurement uncertainties in F_{UV} and the *v* sin *i* determination are shown at the bottom left of the plot. A red cross is shown to represent the parameters belonging to our best-fit model, while the grey shaded region shows the 1-sigma modeling region based on chi-squared fitting transformed from Figure 4. Our radiative-transfer models take T_p as the starting point rather than T_{eff}, and we show a conversion between the two in the inset.

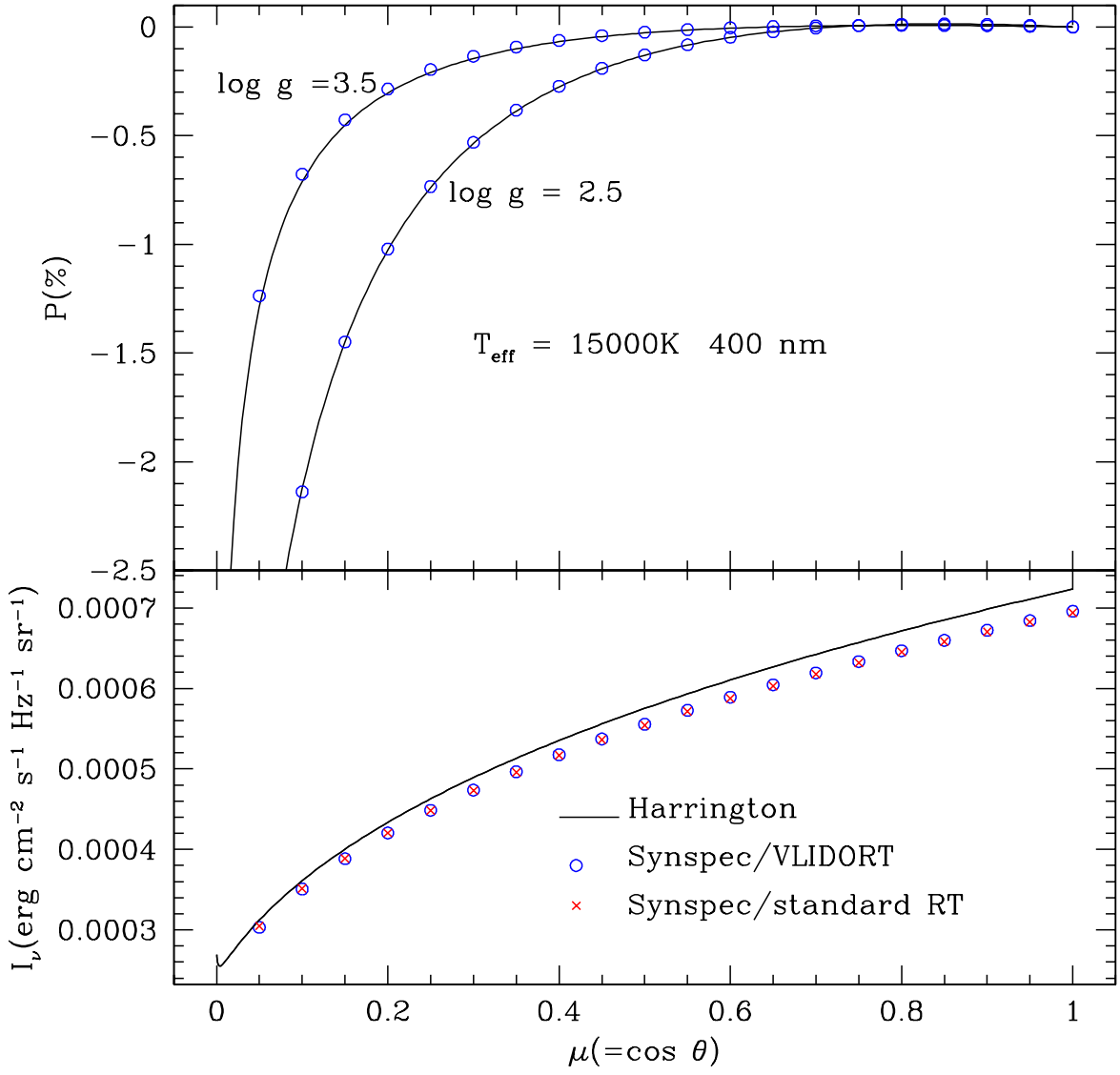

Supplementary Figure 4 | Comparison of SYNSPEC/VILIDORT with the results of Harrington.

Comparison of our SYNSPEC/VLIDORT radiative transfer with results from Harrington[17] for a TLUSTY model with T_{eff} = 15000 K and two different gravities at a wavelength of 400 nm. The top panel shows Harrington's results (solid line) and the SYNSPEC/VLIDORT results (blue circles) for polarization as a function of μ. The bottom panel shows specific intensities (at log g = 3.5 only). The intensities from Harrington are a little higher than those from SYNSPEC, but the SYNSPEC/VLIDORT results agree very well with intensities from SYNSPEC's standard radiative transfer (red crosses).

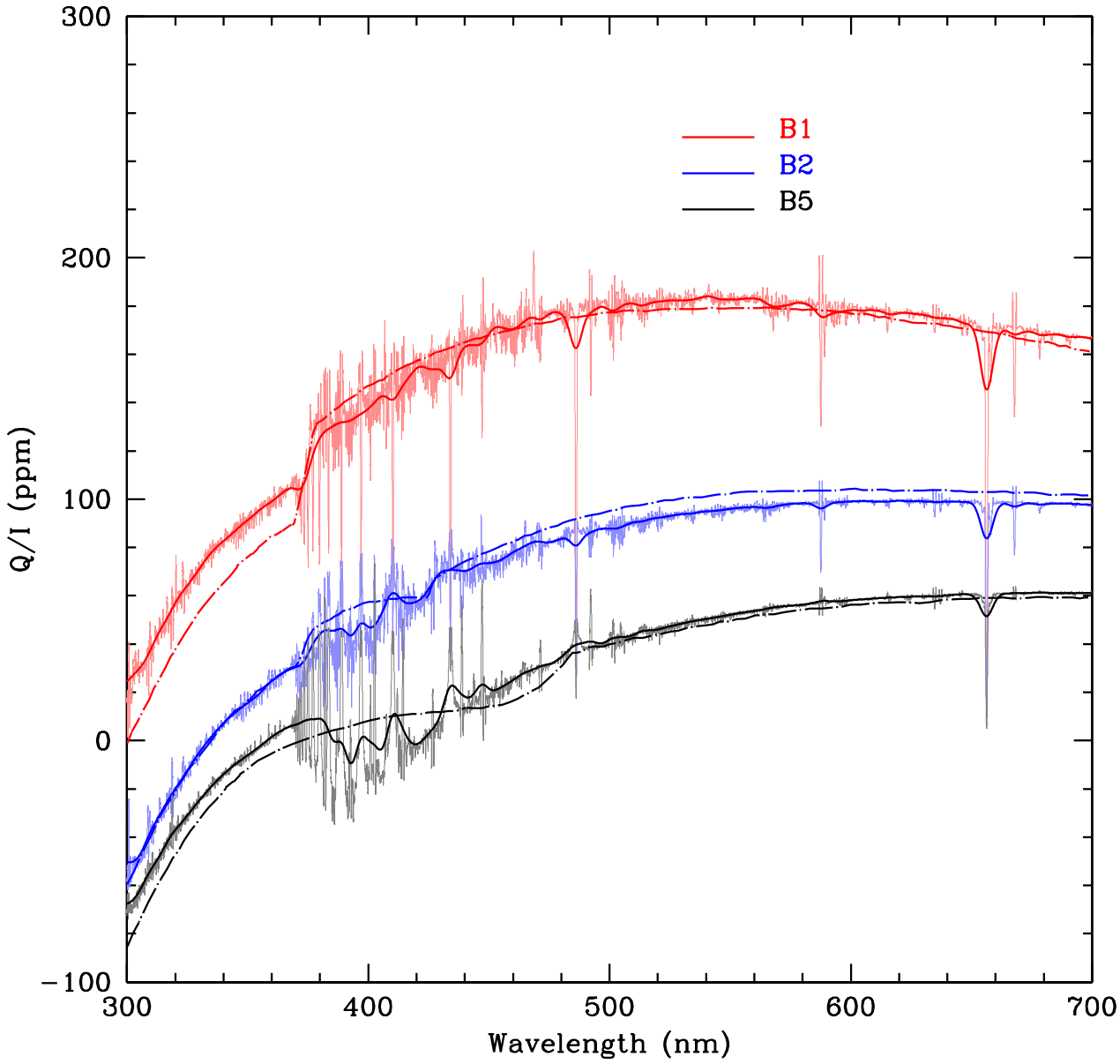

Supplementary Figure 5 | Comparison of SYNSPEC/VILIDORT with the results of Sonneborn.

Polarization for rapidly rotating B stars with ω/ω_c = 0.95 and inclination 90 degrees as calculated by our modeling code (solid lines) compared with results by Sonneborn[8] (dot-dashed lines). Our modeling produces results at high spectral resolution shown by the light colored line here. The heavy line shows the smoothed data. Smoothed values like this are used in Figure 3, but the full resolution of the models is used as input to the bandpass model to facilitate the comparison with observation in Figure 4.

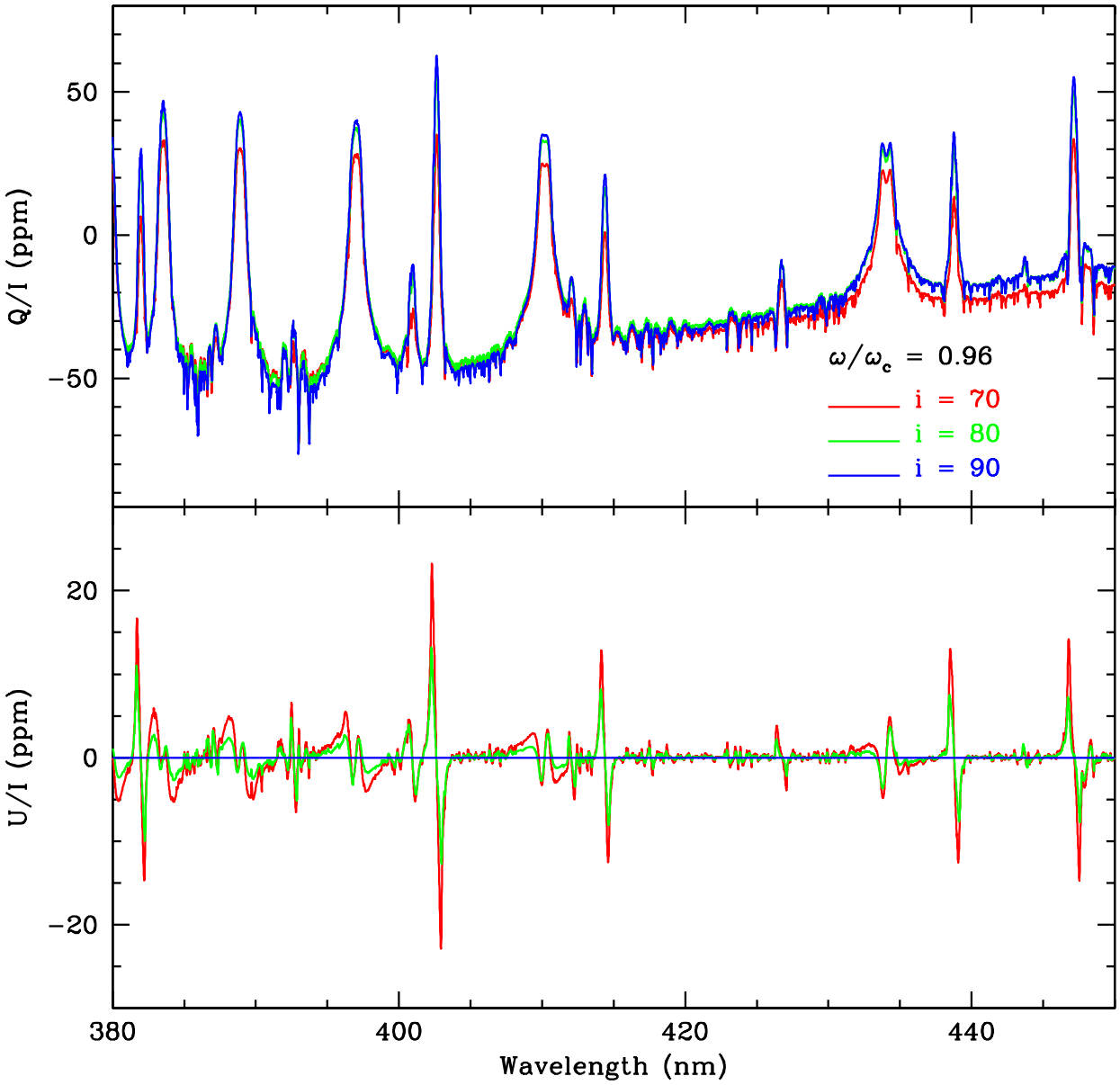

Supplementary Figure 6 | A demonstration of the Öhman Effect in the range 380 to 450 nm for Regulus.

The region of the spectrum from 380 to 450 nm corresponding to polarization models of Regulus for ω/ω_c = 0.96 and inclinations of 70, 80 and 90 degrees. Both Q/I and U/I are shown. It can be seen that the polarization across spectral lines is more sensitive to differences in inclination, at high inclinations, than is the broadband polarization shown in Figure 3.

Supplementary Table 1 | Modeled effective wavelengths and polarization corrections by band.

Spec Type /Star	425SP		SDSS g'		SDSS r' (b)*		SDSS r' (r)		PlanetPol**	
	λ (nm)	Eff. (%)	λ (nm)	Eff. (%)	λ (nm)	Eff. (%)	λ (nm)	Eff. (%)	λ (nm)	Eff. (%)
B0	387.5	45.2	459.1	87.7	595.7	85.3	616.8	81.4	735.0	91.5
A0	397.1	54.7	462.2	88.6	596.6	85.1	618.3	81.1	745.4	92.3
F0	396.3	53.9	466.2	89.6	598.3	84.8	620.8	80.7	753.8	93.0
G0	395.0	52.5	470.7	90.6	599.9	84.5	623.0	80.2	760.5	93.5
K0	396.8	54.2	474.4	91.6	601.0	84.3	624.5	80.0	765.6	93.9
M0	399.6	57.0	477.5	92.0	604.6	83.7	629.3	79.1	791.4	95.1
M5	399.5	56.9	477.3	91.7	605.4	83.5	630.4	78.9	804.4	95.6
Regulus	392.5	50.8	461.0	88.2	596.7	85.1	618.3	81.1	740.9	91.9

Notes: * Tabulated for B0 to M5 are the values associated with the BNS modulator, the efficiencies using the Micron Technologies modulator are systematically higher by ~1.5%.

** The B0 to M5 models shown for PlanetPol are those given by Hough et al.[13]. Whereas we linearly interpolate for intermediate spectral types observed with HIPPI, PlanetPol processing used the closest model. For Regulus we have recreated the PlanetPol bandpass model and run it with the Regulus stellar model. Note that this model goes to 1000 nm, whereas the PlanetPol bandpass extends beyond this to 1050 nm, albeit with very little sensitivity at the additional wavelengths.

Supplementary Table 2 | High-polarization standards observed for position angle calibration.

Star (HD)	p (%)	θ (deg)	Ref	Observations per Run			
				May 2014	Feb 2016	Jun 2016	Dec 2016
84810	1.6	100.0	[32,57]	0	0	0	2
80558	3.3	161.8	[32]	0	1	0	1
147084	4.3	32.0	[58,59]	1	1	1	0
154445	3.4	90.1	[32,57,59]	2	0	1	0
160529	7.0	20.4	[32,57]	1	0	0	0
187929	1.8	93.8	[32]	1	0	0	0

Supplementary Table 3 | Low-polarization standards and their assigned values in each band.

Star	Q/I (ppm)	U/I (ppm)
425SP		
Sirius	0.7 ± 0.6	-1.9 ± 0.2
β Hyi	-1.5 ± 1.1	-5.7 ± 0.4
β Vir	3.4 ± 1.4	-0.1 ± 1.4
g'		
Sirius	0.7 ± 0.6	-1.9 ± 0.2
β Hyi	-1.5 ± 1.1	-5.8 ± 0.4
β Vir	3.4 ± 1.4	-0.1 ± 1.4
r' (b)		
Sirius	0.7 ± 0.6	-1.9 ± 0.2
β Leo	0.8 ± 1.1	2.3 ± 1.1
α Ser	-2.4 ± 0.9	4.0 ± 1.0
r' (r)		
Sirius	0.7 ± 0.6	-1.9 ± 0.2
β Vir	3.4 ± 1.4	-0.1 ± 1.4
*PP**		
β Vir	3.3 ± 1.4	-0.1 ± 1.4
β Leo	0.8 ± 1.1	2.2 ± 1.1
α Ser	-2.3 ± 0.9	3.9 ± 1.0

Notes: * Values for PlanetPol band represent the original measurements from Bailey et al.[15]; these were used only to derive the values in other bands, not for the corrections themselves.

In the case of those stars observed with PlanetPol, the formal 1-sigma errors are propagated from the internal measurement uncertainties (standard deviations), whilst for the other two the errors are defined by the uncertainty in the interstellar polarization with distance trend used to determine *Q/I* and *U/I*.

Supplementary Table 4 | Observations of low-polarization standards for TP calibration.

Star	Band	Date	Time (UT)	Sky* (D/S)	Exp (s)	Q/I (ppm)	U/I (ppm)
β Leo	r' (b)	2014-05-11	13:39:36	S	2560	-22.4 ± 3.5	-51.9 ± 3.1
α Ser	r' (b)	2014-05-11	15:49:02	S	2560	-1.4 ± 2.7	-59.7 ± 2.8
β Leo	r' (b)	2014-05-12	08:43:20	S	2560	-31.7 ± 2.8	-67.3 ± 2.7
May 2014 – r' (b)					**TP:**	**-17.6 ± 12.7**	**-60.3 ± 5.2**
Sirius	425SP	2016-02-26	13:44:25	S	320	-19.6 ± 2.9	-1.2 ± 3.1
Sirius	425SP	2016-02-28	09:48:04	S	320	-26.4 ± 1.6	-2.8 ± 1.6
β Vir	425SP	2016-02-29	14:41:40	S	1280	-11.6 ± 8.7	19.0 ± 10.0
Feb 2016 – 425SP					**TP:**	**-24.5 ± 2.9**	**-2.0 ± 1.4**
Sirius	g'	2016-02-26	09:55:36	-	320	-18.9 ± 1.0	1.6 ± 1.0
Sirius	g'	2016-02-26	13:46:26	S	320	-18.5 ± 1.9	4.4 ± 2.2
β Vir	g'	2016-02-26	17:37:01	S	640	-21.0 ± 6.4	5.4 ± 7.1
Sirius	g'	2016-02-27	09:40:23	S	280	-27.6 ± 3.9	6.3 ± 3.6
Sirius	g'	2016-02-28	09:31:20	S	320	-17.1 ± 1.1	4.4 ± 1.1
β Vir	g'	2016-06-25	08:43:24	S	640	-19.3 ± 9.1	0.2 ± 9.3
β Vir	g'	2016-06-25	09:09:42	S	640	-25.2 ± 6.8	11.7 ± 7.6
β Hyi	g'	2016-06-25	14:18:17	S	640	-13.9 ± 7.8	-11.5 ± 10.3
β Hyi	g'	2016-06-25	16:42:10	S	640	-24.6 ± 4.2	4.6 ± 4.4
Feb 2016 – g'					**TP:**	**-18.7 ± 5.9**	**3.2 ± 4.5**
Sirius	r' (r)	2016-02-27	13:27:31	D	320	-10.6 ± 2.4	-2.9 ± 2.3
β Vir	r' (r)	2016-02-27	16:08:20	S	1280	-11.1 ± 4.8	8.3 ± 5.8
Sirius	r' (r)	2016-03-01	13:42:45	S	320	-9.4 ± 1.4	-3.8 ± 1.5
Feb 2016 – r' (r)					**TP:**	**-9.8 ± 1.2**	**-3.0 ± 1.2**
Sirius	425SP	2016-11-30	17:29:39	S	320	-29.3 ± 3.7	15.8 ± 3.9
β Hyi	425SP	2016-12-01	10:17:47	S	640	-28.2 ± 12.6	18.4 ± 12.8
Sirius	425SP	2016-12-01	15:36:42	D	320	-20.2 ± 2.5	-1.5 ± 2.1
Sirius	425SP	2016-12-07	17:35:21	S	320	-28.8 ± 4.9	4.3 ± 8.2
Dec 2016 – 425SP					**TP:**	**-23.9 ± 4.0**	**2.7 ± 4.3**
β Hyi	g'	2016-11-30	11:08:40	S	640	-30.0 ± 6.3	-4.5 ± 6.2
Sirius	g'	2016-11-30	17:43:01	S	320	-26.0 ± 1.8	1.3 ± 1.8
Sirius	g'	2016-12-02	15:39:03	D	320	-24.1 ± 1.1	0.3 ± 1.2
Dec 2016 – g'					**TP:**	**-24.8 ± 0.9**	**0.4 ± 1.0**
Sirius	r' (b)	2016-12-04	14:00:32	S	640	-23.2 ± 2.9	6.5 ± 3.4
Sirius	r' (b)	2016-12-05	15:57:56	S	640	-15.2 ± 2.0	-3.4 ± 2.2
Dec 2016 – r' (b)					**TP:**	**-17.9 ± 3.6**	**-0.3 ± 4.2**

Notes: * S indicates full sky subtraction, D indicates dark subtraction only, - indicates no subtraction applied.

The data have been bandpass corrected and rotated into the equatorial frame.

The stated errors in the individual observations are the internal standard deviations of the measurements. For the TP determination we use either the root-mean-square of the errors propagated in taking the mean of the individual measurements, or the error-weighted mean of the scatter (standard deviation) in the individual measurements, whichever is greater.

Supplementary Table 5 | Observations of Regulus.

Date	Time (UT)	Exp (s)	Q/I (ppm)	U/I (ppm)	p (ppm)	θ (deg)
Regulus – 425SP						
2016-02-28	12:55:51	2560	31.7 ± 3.5	-4.5 ± 2.5	32.0 ± 3.0	176 ± 2
2016-12-01	17:09:59	2560	22.4 ± 4.7	-8.4 ± 4.9	23.9 ± 4.8	170 ± 6
Regulus – g'						
2016-02-26	14:54:57	1280	12.1 ± 6.2	12.7 ± 5.0	17.5 ± 5.6	23 ± 9
2016-03-01	13:00:15	1600	8.8 ± 6.0	2.2 ± 4.7	9.1 ± 5.3	7 ±15
2016-12-02	16:28:40	960	11.3 ± 2.0	-1.4 ± 1.9	11.4 ± 2.0	176 ± 5
Regulus – r' (b)						
2014-05-11	08:27:17	2080	-16.6 ±12.8	7.6 ± 5.7	18.3 ± 9.3	78 ±11
2016-12-04	14:00:32	1600	-26.8 ± 8.3	14.7 ± 8.4	30.6 ± 8.3	76 ± 8
Regulus – r' (r)						
2016-02-27	14:11:23	2560	-27.3 ± 2.4	15.3 ± 2.4	31.3 ± 2.4	75 ± 2
2016-03-01	14:42:24	2560	-25.3 ± 1.7	14.1 ± 1.8	28.9 ± 1.8	76 ± 2
Regulus – PP						
2005-04-26	21:16:53	1440	-34.8 ± 1.1	12.5 ± 1.0	37.0 ± 1.0	80 ± 1
2006-02-20	04:59:35	1440	-33.4 ± 1.1	15.2 ± 1.1	36.7 ± 1.1	78 ± 1
HD 99028 – g'						
2016-02-26	14:54:57	1280	6.8 ± 5.4	-3.8 ± 5.4	7.8 ± 5.4	166 ±20

Notes: Values are post application of the bandpass model; position angle calibration and TP subtraction and the uncertainties include the errors associated with those operations. Also included are observations of the interstellar control star HD 99028.

The errors in *Q/I* and *U/I* are the root-mean-square errors propagated from the error-weighted mean of the individual observations. The errors in *p* and θ are propagated from those in *Q/I* and *U/I*.

Supplementary Table 6 | Control stars used for interstellar polarization angle determination, and the adopted interstellar polarization for Regulus in the g' band.

Star (HD)	Pos (RA, Dec)	Band	d (pc)	p (ppm)*	θ (deg)	Wt	Ref
81797	09.46h, -08.7°	g'	55.3	8.8±3.7	171±12	0.34	[26]
97603	11.24h, +20.5°	PP	17.9	3.7±2.4	159±23	0.49	[15]
97633	11.24h, +15.4°	PP	50.6	6.9±2.7	25±13	0.53	[15]
99028	11.40h, +10.5°	g'	23.7	7.9±5.4	166±20	0.46	New
102870	11.84h, +01.8°	PP	10.9	3.3±1.4	179±10	0.22	[15]
Regulus	**10.14h, +12.0°**	**g'**	**24.3**	**6.3±1.4**	**175±12**		

Notes: * The *p* given here for the control stars is an undebiased value; and the error is the internal standard deviation of the measurement, propagated from *Q/I* and *U/I* To calculate *p/d* and thus the scatter used as the error in the determined interstellar polarization of Regulus, *p* is debiased as $\hat{p} = \sqrt{p^2 - {\sigma_p}^2}$. See the text for the method of calculating interstellar *p* for Regulus.

Supplementary Table 7 | Combined Regulus measurements before and after interstellar subtraction, and after rotation corresponding to the determined position angle.

Error Weighted Observations				
Band	**Q/I**	**U/I**	**p**	**θ**
425SP	28.4 ± 2.8	-5.3 ± 2.2	28.8 ± 2.5	175 ± 2
g'	11.1 ± 1.8	0.7 ± 1.7	11.2 ± 1.7	2 ± 4
r' (b)	-23.8 ± 7.0	9.8 ± 4.7	25.8 ± 5.8	79 ± 6
r' (r)	-26.0 ± 1.4	14.5 ± 1.4	29.7 ± 1.4	75 ± 1
PP	-34.1 ± 0.8	13.7 ± 0.7	36.8 ± 0.8	79 ± 1
After Interstellar Subtraction				
Band	**Q/I**	**U/I**	**p**	**θ**
425SP	22.2 ± 3.1	-4.3 ± 2.3	22.7 ± 2.7	175 ± 3
g'	4.9 ± 2.3	1.7 ± 1.8	5.2 ± 2.0	10 ±10
r' (b)	-29.8 ± 7.1	10.8 ± 4.7	31.7 ± 5.9	80 ± 5
r' (r)	-31.9 ± 1.9	15.4 ± 1.5	35.4 ± 1.7	77 ± 1
PP	-39.5 ± 1.5	14.6 ± 0.9	42.1 ± 1.2	80 ± 1
After Rotation into the Axial Frame				
Band	**Q_r/I**	**U_r/I**	**p**	**θ_r**
425SP	-22.3 ± 2.4	-3.9 ± 3.0	22.7 ± 2.7	95 ± 4
g'	-4.0 ± 1.9	-3.3 ± 2.2	5.2 ± 1.4	110 ±11
r' (b)	31.7 ± 5.2	0.5 ± 6.7	31.7 ± 6.0	0 ± 6
r' (r)	35.3 ± 1.6	-3.0 ± 1.9	35.4 ± 1.8	178 ± 2
PP	42.1 ± 1.1	0.5 ± 1.4	42.1 ± 1.3	0 ± 1

Notes: The errors in *Q/I* and *U/I* are the root-mean-square errors propagated from the error-weighted mean of the individual observations; those after interstellar subtraction incorporate the error in the determined interstellar polarization as a root-mean-square addition. The errors in *p* and θ are propagated from those in *Q/I* and *U/I*.

Supplementary Table 8 | Adopted and final parameters for Regulus.

Adopted Stellar Parameters		*Notes/References*
$v \sin i$ (km/s)	318 ± 8	*a*, [37-40]
V (mag)	1.35 ± 0.02	[60]
d (pc)	24.3 ± 0.2	[31]
M_V (mag)	-0.58	*a*
Interstellar Medium		
λ_{max} (nm)	470	[27]
p_{max} (ppm)	6.3 ± 1.4	*a*, [28]
θ_{ISM} (deg)	175 ± 12	*b*, [28]
Polarimetric Determination		
θ_R (deg)	79.5 ± 0.7	*c*
Modeling Determination		
i (deg)	80.0 (> 76.5)	*c*
ω/ω_c	$0.965\ ^{+0.006}_{-0.008}$	*c*
log g_p	$3.992\ ^{+0.022}_{-0.026}$	*c*
log g_{eq}	$3.333\ ^{+0.095}_{-0.099}$	*c*
T_p (K)	$14375\ ^{+215}_{-181}$	*c*
T_{eq} (K)	$11060\ ^{+138}_{-140}$	*c*
T_{eff} (K)	$12626\ ^{+190}_{-163}$	*c*
Other Derived Physical Parameters		
Mass (M_{Sun})	$3.72^{+0.56}_{-0.47}$	*d*
r_p (r_{Sun})	$3.22^{+0.29}_{-0.25}$	*d*
r_{eq} (r_{Sun})	$4.22^{+0.35}_{-0.31}$	*d*
P_{rot} (*d*)	$0.662^{+0.046}_{-0.042}$	*d*
log (L/L_{Sun})	$2.520^{+0.076}_{-0.075}$	*d*
v_e/v_c	$0.844^{+0.015}_{-0.017}$	*d*

Notes: (a) calculated based on available data, (b) one additional measurement was added to those available in the literature to calculate this parameter, (c) determined from measurements and models first presented in this work, (d) calculated based on the determined and adopted parameters.

See the Methods section of the text for a description of how the errors were determined for each quantity. Specifically, for data not taken directly from the literature, this information can be found in the sections headed Interstellar polarization subtraction, Determination of Regulus' rotation-axis position angle, Determination of projected equatorial rotational velocity, Constraining stellar parameter space, and Regulus final parameters.